INTERFEROMETRIC MAPPING OF MAGNETIC FIELDS: THE MASSIVE STAR-FORMING REGION G34.4+0.23 MM

P. C. Cortes
Departamento de Astronomía, Universidad de Chile, Casilla 36-D Santiago, Chile

R. M. Crutcher
Astronomy Department, University of Illinois at Urbana-Champaign, IL 61801

D. S. Shepherd[1]
National Radio Astronomy Observatory, P.O. Box O, 1003 Lopezville Road, Socorro, NM 87801

AND

L. Bronfman
Departamento de Astronomía, Universidad de Chile, Casilla 36-D Santiago, Chile

ABSTRACT

We report millimeter interferometric observations of polarized continuum and line emission from the massive star-forming region G34.4. Polarized thermal dust emission at 3 mm wavelength and CO $J = 1 \rightarrow 0$ line emission were observed using the Berkeley-Illinois-Maryland Association (BIMA) array. Our results show a remarkably uniform polarization pattern in both dust and in CO $J = 1 \rightarrow 0$ emission. In addition, the line emission presents a consistent uniform polarization pattern over most of the velocity channel maps. These uniform polarization patterns are aligned with the north-south main axis of the filament between the main millimeter source (MM) and the ultracompact H II region, which are the central sources in G34.4, suggesting a magnetic field orthogonal to this axis. This morphology is consistent with a magnetically supported disk seen roughly edge-on.

Subject headings: ISM: magnetic fields — stars: formation

Online material: color figure

1. INTRODUCTION

It is generally accepted that magnetic fields play an important role in the process of star formation; magnetic fields are involved in cloud support, fragmentation, and transfer of angular momentum. However, the magnetic field is the least-observed physical quantity involved in such processes. Magnetic field observations of molecular clouds are divided into measurements of the line-of-sight component of the magnetic field strength through the Zeeman effect and observations of the field in the plane of the sky through linear polarization of dust emission and spectral-line emission. The alignment of dust grains by a magnetic field is physically complicated and is still a matter of intense research. It is accepted, however, that aligned dust grains will produce polarized emission perpendicular to the projection of the magnetic field onto the plane of the sky. For a recent review of alignment theories see Lazarian (2007).

It has been suggested that spectral-line linear polarization arises from molecular clouds under anisotropic conditions, such as large velocity gradients (or LVGs; Goldreich & Kylafis 1981). The prediction suggests that a few percent of the linearly polarized radiation should be detected from molecular clouds and circumstellar envelopes in the presence of a magnetic field. This polarization will be either parallel or perpendicular to the projection of the field onto the plane of the sky. To obtain a qualitative understanding about this effect, consider the CO molecule emitting unpolarized radiation. Under a magnetic field, a CO molecule will develop a small splitting in its rotational, J, energy levels. These magnetic sublevels will produce radiation components labeled σ for the $|M - M'| = 1$ transitions, and π for the $|M - M'| = 0$ transitions, where both components can be linearly polarized either perpendicular or parallel to the magnetic field. If the gas behaves under isotropic conditions (e.g., no velocity gradients) for any direction the σ and π will populate equally, so the radiation components emerging from the radiative decays of these states will combine to give zero net polarization. Now on the other hand, large velocity gradients present in molecular clouds will produce anisotropies in the optical depths for the CO molecular transitions at different directions. If the velocity gradients are smaller in directions parallel to the magnetic field than in those perpendicular to the field, the optical depths parallel to the field will be larger than the optical depths perpendicular to them. Therefore, the escape of radiation involved in de-exciting the upper J state will be then reduced more in directions along the field lines than in directions perpendicular to them, which will lead to populations of the magnetic σ substates that are larger than the populations of the π substates due to the difference in the angular distributions of both radiation components. The angular distribution of the σ component peaks in directions along the field lines, whereas the π component peaks in directions perpendicular to the magnetic field. In this way, the rate of de-excitation for σ will have a larger decrease, due to photon trapping, than the rate of de-excitation for the π radiation component. Because in this picture the σ component will have a larger population, its emission will be stronger relative to the π component, giving rise to a small amount of

[1] The National Radio Astronomy Observatory is a facility of the National Science Foundation operated under cooperative agreement by Associated Universities, Inc.

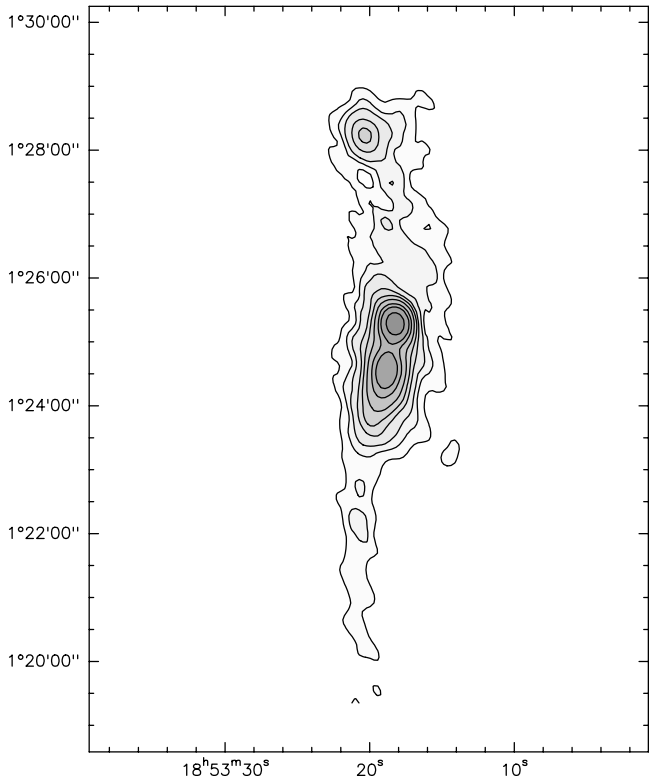

FIG. 1.—Filament which includes the G34.4+0.23 MM source. This figure was taken from data in Faúndez et al. (2004), who observed the region at 1.2 mm with the SEST. We can clearly see the flattened and elongated morphology of the cloud.

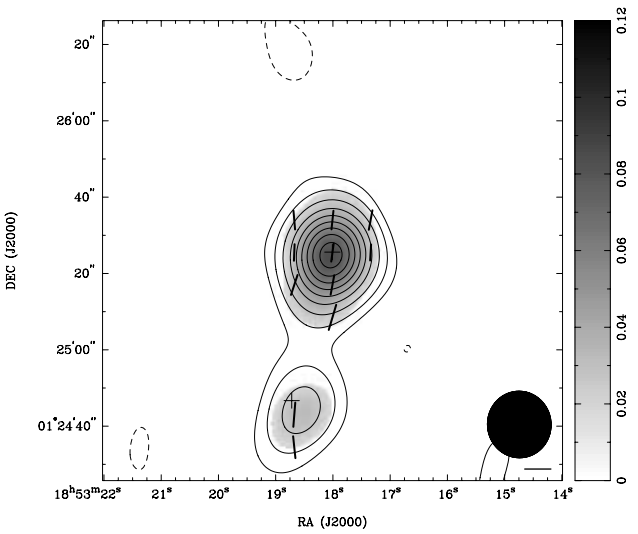

FIG. 2.—Continuum polarization map at 3 mm. This map consists of an intensity-only map (or Stokes I) shown by contours at levels of -3, 3, 6, 10, 15, 20, 25, 30, 35, and 40 σ where $\sigma = 6$ mJy beam^{-1}. The beam is indicated by the black filled circle at the bottom right corner of the map. The gray-scale map indicates the polarized flux $[(U^2 + Q^2)^{1/2}]$, also measured in Jy beam^{-1}. The line segments show the polarization P.A. and the fractional polarization, which is indicated by the length of the line. The bar at the bottom right, below the beam, shows a fractional polarization scale of 0.4. The plus signs indicate the location of the MM and the UC H II regions.

linear polarization in the CO emission with the polarization of the σ component, or perpendicular to the magnetic field. The effect was first detected by Glenn et al. (1997) for the CS molecules, while Greaves et al. (1999) detected CO polarized emission for ($J = 2 \rightarrow 1$) and ($J = 3 \rightarrow 2$) transitions.

In order to efficiently map polarized emission and infer detailed information about the magnetic field morphology, high-resolution observations are required. The BIMA millimeter interferometer has been used previously to obtain high-resolution polarization maps in several star-forming cores (Lai 2001; Lai et al. 2002, 2003; Cortes et al. 2005, 2006; Cortes & Crutcher 2006). These previous results show fairly uniform polarization morphologies over the main continuum sources, suggesting that magnetic fields are strong, and therefore cannot be ignored by star formation theory. However, the number of star formation regions with maps of magnetic fields remains small, and every new result is statistically significant. In this work we present polarization maps of the massive star-forming region G34.4, obtained with the BIMA array. We measured continuum polarization at 3 mm and CO $J = 1 \rightarrow 0$ line polarization, obtaining interferometric maps for both line and continuum. The remainder of this paper is divided into five sections. Section 2 reviews information about the source, § 3 describes the observation procedure, § 4 presents the results, § 5 gives the discussion, and § 6 the conclusions and summary.

2. SOURCE DESCRIPTION

G34.4 is a newly discovered massive star-forming region. It is associated with the IRAS 18507+0121 point source, which is located at 3.9 kpc from the Sun, having a $v_{\rm lsr} = 57$ km s^{-1}. Toward the IRAS 18507+0121 point source, Bronfman et al. (1996) detected strong CS($J = 2 \rightarrow 1$) emission with broad line wings that suggested massive star formation. The source is roughly 11′ from the H II region complex G34.3+0.2 (Molinari et al. 1996). Observations with the 45 m Nobeyama radio telescope at a resolution of 16″ of HCO^+, $H^{13}CO^+$, CS, and $C^{34}S$ were presented by Ramesh et al. (1997). Their modeling showed that the observed line profiles are representative of a collapsing warm (22 K) core with a mass of 800 $M_\odot$, hidden behind a ≈4 K cold screen of about 200 $M_\odot$. This region is also associated with H_2O maser emission (Scalise et al. 1989; Palla et al. 1991; Miralles et al. 1994) and CH_3OH maser emission (Schutte et al. 1993; Szymczak & Kus 2000). Faúndez et al. (2004) observed this region in the continuum at 1.2 mm with the Swedish-ESO Submillimetre Telescope (SEST) and derived a mass of 2×10^3 $M_\odot$. Shepherd et al. (2004) performed the first interferometric observations with Owens Valley Radio Observatory (OVRO) of the 3 mm continuum, $H^{13}CO^+$($J = 1 \rightarrow 0$), and SiO($v = 0$, $J = 2 \rightarrow 1$). They detected two compact molecular cores along a north-south filament, separated by ∼40″ (see Fig. 1). They also presented near-infrared observations at J, H, and K' ($\lambda_c = 1.25$, 1.65, and 2.1 μm, respectively). The central source in Figure 2 (labeled G34.4+0.23 MM) showed no trace of NIR emission, but the southern source seemed to be associated with a NIR cluster of young stars and an ultracompact H II region. Based on the emission from warm dust and the lack of NIR emission, the central source was suggested to be a massive protostar. From the Very Large Array (VLA) archive, marginal emission (0.7 mJy) of 6 cm radio continuum was detected from this source (Shepherd et al. 2004). Rathborne et al. (2005) made a multiwavelength study of this region. They observed continuum emission at 1.2 mm, and 850, 450, and 350 μm by using IRAM, James Clerk Maxwell Telescope (JCMT), and the Caltech Submillimeter Observatory (CSO), respectively. They also obtained archival data from *Spitzer Space Telescope* at 2.4, 8, 4.5, and 3.6 μm and produced combined maps of infrared continuum emission. Their data agree well with previous observations and positioned the infrared sources at the center of the millimeter and submillimeter emission. In a

recent study, Shepherd et al. (2007) presented a detailed study of the G34.4 region. They discovered five massive outflows from two of the existing cloud cores in G34.4. Three outflows are centered near the ultracompact (UC) H II region while the remaining two are centered at the MM core. By using mid-IR data from *Spitzer*, Shepherd et al. (2007) identified a total of 31 young stellar objects (YSOs) in the G34.4 complex with a combined mass of $\sim$127 $M_\odot$ plus an additional 22 sources that might be cluster members based on strong 24 μm emission.

3. OBSERVATION PROCEDURE

We observed G34.4+0.23 MM in 2004 May in the 3 mm continuum and the CO $J = 1 \rightarrow 0$ molecular line (at 115 GHz); one track with the BIMA array in D configuration (at a resolution of 16″) was obtained. The digital correlator was set up to observe both the continuum and the CO $J = 1 \rightarrow 0$ line simultaneously. The 750 MHz wide lower side band was combined with 700 MHz from the upper side band to map the continuum emission, leaving a 50 MHz window for the CO line observation (at a resolution of 2.06 km s^{-1}). The 50 MHz window for CO was cut from the continuum window to avoid contamination of the continuum by the CO line and reduced independently. In order to detect circular polarization, a quarter-wave plate was placed in front of the single receiver at each BIMA antenna to select either right (R) or left (L) circular polarization. A second quarter-wave plate grooved orthogonally to the first was alternately switched into the signal path to sequentially observe both circular polarizations. Switching between polarizations was sufficiently rapid (every 11.5 s) to give essentially identical *u-v* coverage. Cross-correlating the R and L circularly polarized signals from the sky gave RR, LL, LR, and RL correlations for each interferometer baseline, from which maps of the four Stokes parameters were produced. The quasars 1751+096 and 1743−038 were used as calibrators for G34.4. The instrumental polarization was calibrated by observing the 3C279 quasar, and the "leakages" solutions were calculated from this observation. The calibration procedure is described by Lai (2001). The Stokes images *I*, *U*, *Q*, and *V* were obtained by Fourier transforming the visibility data using a robust weighting scheme (Briggs et al. 1999). Deconvolution in the Stokes *I* cube was done by applying a maximum entropy algorithm to every channel. The MIRIAD (Sault et al. 1995) package was used for data reduction.

4. OBSERVATIONAL RESULTS

4.1. 3 mm *Continuum*

The 3 mm continuum results are shown in Figure 2. The beam has a major axis of 17.6″ and a minor axis of 15.7″. The significance level cutoff chosen for the polarization results is 3 σ, where σ refers to the noise level in the polarized flux image values below 3 σ are blanked in the data analysis process. The strongest feature of the 3 mm continuum result is the main compact source centered at $(\alpha, \delta) = (18^{\rm h}53^{\rm m}18^{\rm s}, 01^\circ25'25'')$; this structure is in agreement with the 3 mm continuum result of Shepherd et al. (2004) at higher resolution and corresponds to their MM (millimeter) core. Some additional structure is seen along the north-south axis of the cloud. However, interferometric observations of equatorial sources can produce *ghost* structures along the north-south axis, due to the strong sidelobes that appear in the synthesized beam at such declinations. In the case of our source, the emission seen south of the MM core appears to be associated with IRAS 18507+0121 [or the UC H II region with a

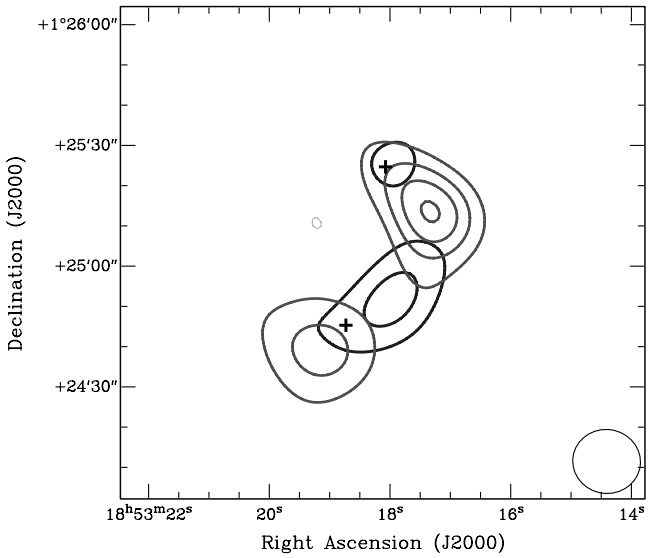

FIG. 3.—Composite plot which superposes the averaged blueshifted lobe (*black contours*) and the redshifted lobe (*gray contours*), plotted as −3, 3, 6, 9, and 12 σ where $\sigma = 0.6$ Jy beam^{-1}. The thick lines represent the positive emission, while the negatives are given by the small gray circle in between both sources. The beam is plotted as a black oval at the bottom right corner. The lobes are calculated using the velocity interval $v = 60$ to $v = 80$ km s^{-1} for the red lobe and $v = 38$ to $v = 54$ km s^{-1} for the blue lobe. As in previous figures, the plus signs represent the MM core and the UC H II region. [*See the electronic edition of the Journal for a color version of this figure.*]

peak emission centered at $(\alpha, \delta) = (18^{\rm h}53^{\rm m}19.5^{\rm s}, 01^\circ24'45'')$], a source that is clearly seen in Figure 1.

The polarization observed in our continuum map is within the MM core and the UC H II region, with the highest polarized flux at the MM core. This source has a peak flux of 273 mJy beam^{-1}, an integrated flux of 290 mJy (calculated over a box of 15″ × 15″ centered at the reference position), and a peak polarized flux *P* of 83 mJy beam^{-1}; the *I* and *P* peaks approximately coincide. The Stokes *I* image shows some filamentary structure along the north-south axis between the MM core and the UC H II region, consistent with the general cloud morphology (see Fig. 1), while the polarized flux is concentrated around the cores. The average position angle (P.A.) of the polarized continuum map is $-8^\circ \pm 5^\circ$, suggesting polarization along the north-south axis of the filament. The fractional polarization seems uniform over both cores, with an average value of 0.3 ± 0.07. However, interferometric observations that do not fully sample the *u-v* plane do not produce reliable fractional polarization results, often overstating the fractional polarization, but not significantly affecting the polarization position angle.

The Shepherd et al. (2004) continuum observations, centered at 90 GHz, yielded a total flux of 56 mJy, about 4 times less than our value. Our observations have an rms noise level of 6 mJy beam^{-1} with an uncertainty in the calibration of 25%, while Shepherd et al. (2004) achieved an rms noise level of 3 mJy beam^{-1} with a calibration uncertainty of 15%. Assuming an error of 3 σ and taking into account the uncertainty in the calibration, the lower limit for our measured flux is 200 mJy. By the same argument, the upper limit for the flux measured by Shepherd et al. (2004) is 75 mJy. The remaining ratio of 2.2 between the two measurements is due mainly to the different frequencies. Emission from a blackbody will produce larger values at higher frequencies in the millimeter part of the electromagnetic spectrum; for example, the flux at 115 GHz will be about twice that at 90 GHz for a 50 K source. The small remaining

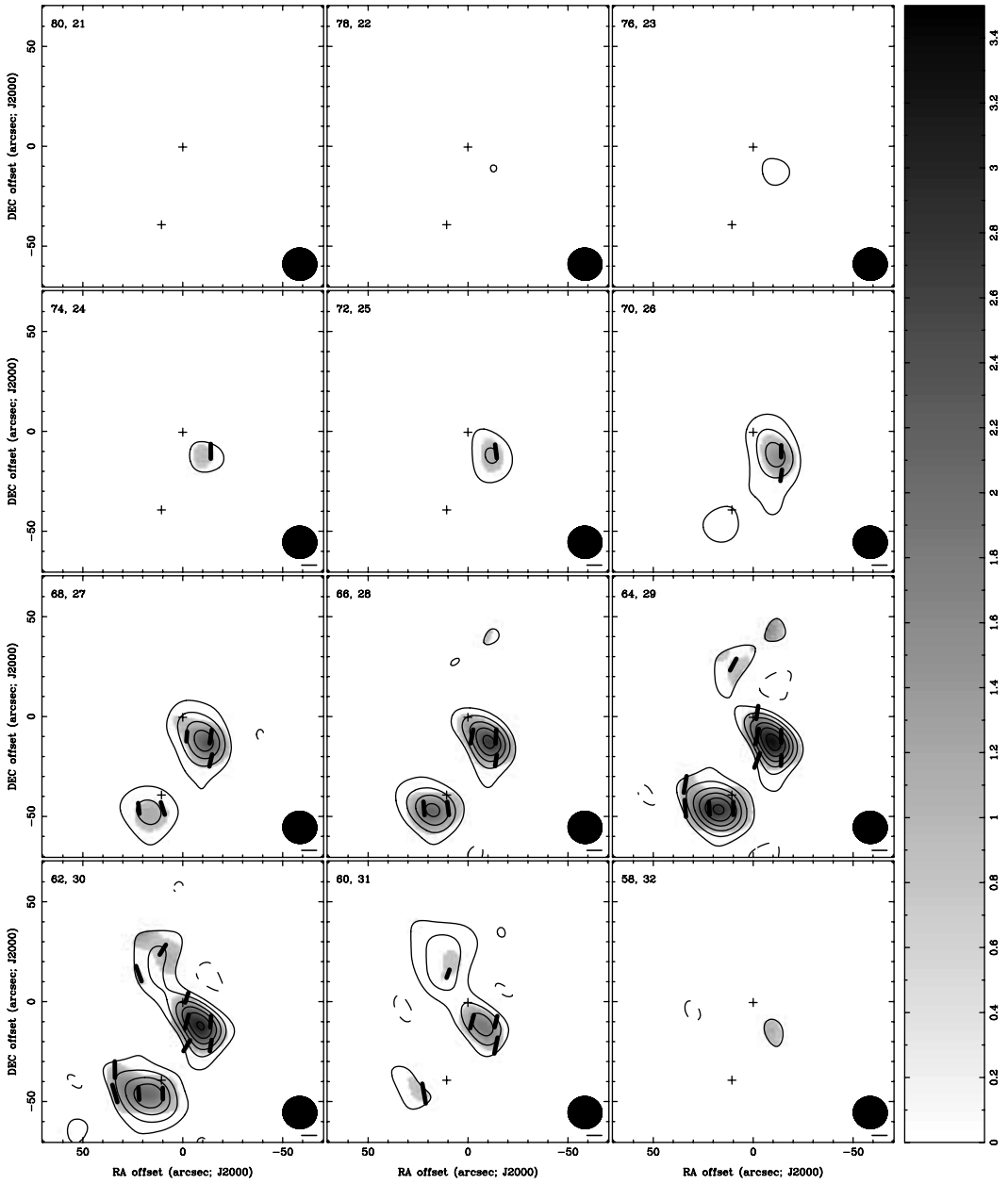

FIG. 4.— Velocity channel maps showing the redshifted velocity component of the emission. The channel maps have velocity and channel number written at the top left corner of each map; the beam is plotted at the bottom right. The Stokes *I* emission is plotted as contours of -3, 3, 6, 9, 12, 15, and 18 σ where $\sigma = 0.7$ Jy beam^{-1}. Polarized flux is shown as gray scale and the line segments represent fractional polarization and P.A. The bar below the beam is the fractional polarization scale of 0.26 and the plus signs show the position of the MM core and of the UC H II region.

difference could be explained by missing flux in the higher resolution interferometric observations of Shepherd et al. (2004) due to missing short spacings in u-v space. Our compact BIMA D array observations have fairly good short-spacing coverage, with shortest baselines of $\sim$9 m, which provides sensitivity up to structures $\sim 60''$ in size.

Emission in the continuum at 3 mm may be contaminated by free-free emission, but that appears not to be the case here. Shepherd et al. (2004) found marginal free-free continuum emission in the 6 cm band that is estimated to be 0.52 mJy at 3 mm. This free-free emission is unpolarized and negligible when compared with our total flux at 3 mm. However, synchrotron emission, which is strongly linearly polarized, could be present. The polarization of synchrotron radiation in the case of a homogeneous magnetic field can achieve a level of 72% for a power-law emission of $n = 0.75$ (Rohlfs & Wilson 2004). The total level of emission found at 6 cm was only 0.7 mJy, which would yield linearly polarized radiation about 0.5 mJy. However, due to the ν^{-n} scaling law for synchrotron emission, its contribution to the polarized flux at the 3 mm band is negligible. Therefore, the contamination in our polarized flux appears to be minimal. This strongly suggests that we are seeing only polarized emission from dust.

4.2. CO $J = 1 \rightarrow 0$

The Rathborne et al. (2005) work featured spectra with broad line widths, suggesting evidence for outflow emission toward the MM core; this was later confirmed by Shepherd et al. (2007), who discovered five massive outflows. Our CO $J = 1 \rightarrow 0$ emission shows similar features for outflow emission; the

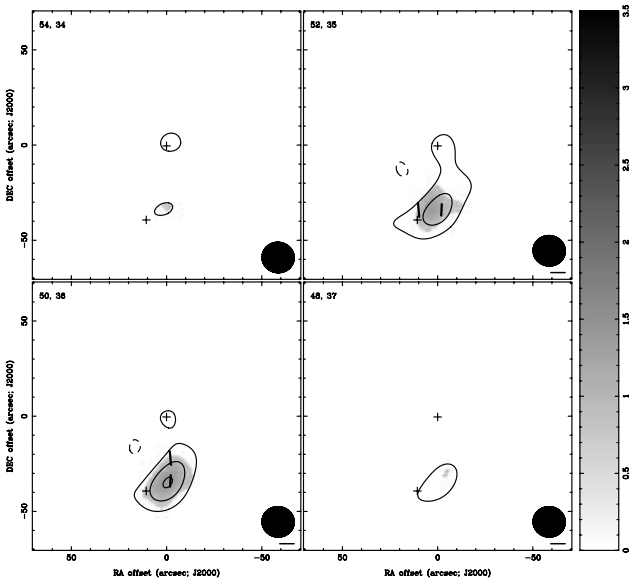

FIG. 5.—Velocity channel maps showing the blueshifted component of the emission. The channel maps have velocity and channel number written at the top left corner of each map; the beam is plotted at the bottom right. As for Fig. 4, the Stokes I emission is shown as contours of -3, 3, 6, 9, 12, 15, and 18 σ where $\sigma = 0.7$ Jy beam^{-1}. Polarized flux is shown as gray scale and the line segments represent fractional polarization and P.A. The bar below the beam is the fractional polarization scale of 0.26 and the plus signs show the position of the MM core and of the UC H II region.

composite plot in Figure 3 shows the blue and red lobes of the CO $J = 1 \rightarrow 0$ emission. We used approximately the same velocity ranges used by Shepherd et al. (2007) to define the outflow lobes (60–80 km s^{-1} for the red lobe and 38–54 km s^{-1} for the blue lobe). Individual channel maps are shown in Figures 4 and 5 (including the polarization). Considering the larger beam of our BIMA D-array observations, which will smear out the emission, our results are in agreement with the higher resolution observations of Shepherd et al. (2007). Although we did not resolve all of the individual outflows detected by their work, it appears that the massive outflow in the MM core (outflow A) is dominating the emission in our observations. Our peak CO flux is calculated around the MM source, centered at $(\alpha, \delta) = (18^{\rm h}53^{\rm m}17.3^{\rm s}, 01^\circ25'15'')$, and taking a value of $\sim$14 Jy beam^{-1}. Table 1 presents the average P.A. for all channels associated with polarized CO emission. From Table 1 we see polarized emission at higher velocities (105–97 km s^{-1}) and at more intermediate velocities associated with the MM outflow. The polarization is observed to be quite uniform, with an orientation mostly along the north-south axis of the filament, in all velocity channels shown in Figures 4 and 5. The peaks in polarized flux and polarization coverage is around 64–62 km s^{-1}, which coincides with the peaks in CO emission. This uniform polarization pattern is similar to the polarization orientation of our 3 mm continuum results. Taking into consideration that molecular line polarization can be either parallel or orthogonal to the magnetic field, these results reinforce the polarized dust emission results—a magnetic field orthogonal to the main axis of the filament.

5. ANALYSIS

5.1. *Core Mass Estimation*

The G34+0.23 MM column density and mass are estimated from dust emission. We follow the derivation made by Mezger (1994). This derivation uses a parameterized representation of

TABLE 1

AVERAGES OF FRACTIONAL POLARIZATION AND POSITION ANGLES

Channel Number	Velocity (km s^{-1})	$P_{\rm CO}$	$\phi_{\rm CO}$ (deg)
9	104.8	0.4 ± 0.1	−0.2 ± 7.4
10	102.7	0.4 ± 0.1	5.2 ± 7.4
11	100.7	0.4 ± 0.2	3.5 ± 8.8
16	90.5	0.3 ± 0.1	6.4 ± 9.9
17	88.5	0.3 ± 0.1	19.6 ± 9.4
20	82.4	0.3 ± 0.2	−15.1 ± 10.0
24	74.3	0.3 ± 0.1	−4.1 ± 8.8
25	72.2	0.2 ± 0.08	4.9 ± 8.1
26	70.2	0.2 ± 0.05	−1.2 ± 7.1
27	68.2	0.2 ± 0.06	−1.9 ± 6.8
28	66.2	0.2 ± 0.06	−0.4 ± 6.0
29	64.1	0.3 ± 0.07	−2.3 ± 5.7
30	62.1	0.2 ± 0.07	−8.87 ± 6.3
31	60.1	0.2 ± 0.07	−13.7 ± 7.4
32	58.0	0.4 ± 0.2	−12.9 ± 8.0
34	54.0	0.3 ± 0.2	−2.4 ± 9.9
35	51.9	0.2 ± 0.08	0.6 ± 7.8
36	49.9	0.2 ± 0.07	−1.9 ± 7.5
37	47.9	0.2 ± 0.09	−8.8 ± 10.0
40	41.8	0.4 ± 0.2	−4.9 ± 8.1

NOTE.—Values are per channel, of CO ($J = 1 \rightarrow 0$) polarized emission from G34.4.

the dust absorption cross section per H atom. This parameterization follows $\tau_\nu/N_{\rm H} = \sigma_\lambda^{\rm H}$ in cm^2 per H atom, where

$$\sigma_\lambda^{\rm H} = \frac{Z}{Z_\odot} b\left(7\times10^{-21}\lambda_{\mu\rm m}^{-2}\right)\lambda_{\mu\rm m} \geq 100. \quad (1)$$

$Z/Z_\odot = 1$ is the relative metallicity, $\lambda_{\mu\rm m}$ is the wavelength in μm, and b is parameter used to introduce the grain dependence on gas density (Mezger 1994). The b parameter usually takes values of $b = 1.9$ for $n_{\rm H} \leq 10^6$ cm^{-3} and $b = 3.4$ for higher densities. With these considerations, the expressions for the cloud mass and column density are calculated using the expressions derived by Mooney et al. (1995),

$$\frac{N_{\rm H}}{\rm cm^{-2}} = 1.93\times10^{15}\frac{\left(S_{\nu,\rm int}/\rm Jy\right)\lambda_{\mu\rm m}^4}{\left(\theta_s/\rm arcsec\right)^2(Z/Z_\odot)bT}\frac{e^x-1}{x}, \quad (2)$$

$$\frac{M_{\rm H}}{M_\odot} = 4.1\times10^{-10}\frac{\left(S_{\nu,\rm int}/\rm Jy\right)\lambda_{\mu\rm m}^4 D_{\rm kpc}^2}{(Z/Z_\odot)bT}\frac{e^x-1}{x}, \quad (3)$$

where $N_{\rm H} = N({\rm H}) + 2N({\rm H_2})$ is the total hydrogen column density, $S_{\nu,\rm int}$ is the integrated flux density from the source, $\theta_s = (\theta_{s,\rm min}\theta_{s,\rm max})^{1/2}$ is the angular source size, $x = (1.44\times10^4)/(\lambda_{\mu\rm m}T)$ is the $(hc)/(\lambda kT)$ factor for the Planck function, $D_{\rm kpc}$ is the distance to the source in kpc, T is the dust temperature, and b is taken to be $b = 3.4$ to reflect the massive MM core. Shepherd et al. (2004) estimated $T = 50$ K, the value that we use here, as the most likely dust temperature for the MM core. Using the flux of 290 mJy estimated from our 3 mm continuum emission, we obtain a column density of 6×10^{23} cm^{-2} and a total mass of 520 $M_\odot$. Shepherd et al. (2004) obtained a mass of 250 $M_\odot$ (their masses varied up to 650 $M_\odot$ for different values of dust temperature and emissivity).

5.2. *Field Direction*

The general morphology of the G34.4 massive star-forming region is of a filament, where all sources are embedded along

the main axis of the cloud (see Fig. 1 here and maps in Rathborne et al. 2005; Shepherd et al. 2007). This type of morphology appears to be widespread in the interstellar medium (ISM; Faúndez et al. 2004). How this elongated cloud morphology is produced is still an open question; one avenue of research is to understand the dynamical effect of magnetic fields on the gas and dust in these regions. Our dust polarized emission results show a uniform pattern over both the MM core and the UC H II region, with an average P.A. of $-8^\circ \pm 5^\circ$ aligned with the main axis (north-south) of the filament, between the MM core and the UC H II region (see Fig. 2). Polarized emission from dust grains suggests alignment of grains by a magnetic field; the aligned grains will produce polarized emission with P.A.s orthogonal to the projection of the field onto the plane of the sky. Therefore, our observations suggest a magnetic field morphology with field lines orthogonal to the main axis of the filament between the MM core and the UC H II region.

A similar interpretation applies for our CO $J = 1 \rightarrow 0$ observations, shown in Figures 4 and 5 in velocity channel maps. Table 1 shows the average values for the P.A. for all channel maps with their corresponding spatial dispersion. A P.A. average of $-2^\circ \pm 8^\circ$ is calculated for all channels. Figure 6 shows the same plot as Figure 3, but with the polarization map overplotted. The image to the left in each panel shows an average of channels from 80 to 60 km s^{-1} for the red lobe, while the image to the right in each panel shows an average of channels from 54 to 38 km s^{-1}, representing the blue lobe. The average P.A. in the red lobe is $-3^\circ \pm 7^\circ$, while in the blue lobe it is $-3^\circ \pm 9^\circ$, consistent with the average and overall values shown in Table 1. Figure 7 shows panels with spectra from the most intense CO $J = 1 \rightarrow 0$ emission points. These two spectra were obtained from averages of $8''$ boxes around the points $(\alpha, \delta) = (18^{\rm h}53^{\rm m}17.3^{\rm s}, 01^\circ25'15'')$ and $(18^{\rm h}53^{\rm m}19.2^{\rm s}, 01^\circ24'41'')$, which can be easily spotted in Figure 4 at channel map number 30, or at $V = 62$ km s^{-1}, corresponding to the main emission peaks on the map. Superposed onto each spectrum are fractional polarization and P.A. values which are also consistent with Table 1 and with the previous CO $J = 1 \rightarrow 0$ figures. It is interesting to see how the fractional polarization values are fairly constant over most of the CO emission at both spectra, while the P.A. values are well clustered around 0°. The large fractional CO ($J = 1 \rightarrow 0$) polarization values obtained in our observations can be explained, most likely, by missing flux in the Stokes I emission due to incomplete u-v coverage at the shorter baselines of the BIMA D array configuration.

As with the polarized dust emission results, the polarization line segments seem to be well aligned with the filament axis, showing little spatial dispersion over all relevant channels. Cortes et al. (2005) showed that strong large-velocity gradients will produce polarization perpendicular to the magnetic field even if a weak continuum source is present, which seems to be the case in our observations. Therefore, our results for both polarized dust and CO $J = 1 \rightarrow 0$ results suggest a magnetic field orthogonal to the main axis of the filament. Flattened filamentary cores with magnetic field lines perpendicular to their main axis have been observed before. The Schleuning (1998) map of $8' \times 8'$ of the OMC-1 region shows a magnetic field that is not only orthogonal to the main axis of the cloud but also has an hourglass shape. Cortes et al. (2006) made interferometric observations with BIMA toward the NGC 2071 IR star-forming region, finding a magnetic field orthogonal to the main axis of an elongated structure.

It has also been suggested that CO line polarization will, most likely, trace a different environment than dust polarization. Cortes et al. (2005) showed that radiation from the CO $J = 1 \rightarrow 0$ transition will present a maximum amount of fractional polarization when emitted from densities $n_{\rm H_2} \sim 100$ cm^{-3}, which will most likely correspond to cloud envelopes, such as the cold screen proposed by Ramesh et al. (1997), or to outflow extended regions. In the case of G34.4, the data support a magnetic field aligned with the main axis of the cloud even at regions dynamically dominated by the outflows. However, polarized line emission tracing outflows aligned with magnetic fields has been observed (Girart et al. 1999; Cortes et al. 2006). This apparent discrepancy might be explained by the difference in spatial resolution between this work and previous findings; while Cortes et al. (2006) interferometric observations achieved a resolution of $4''$ from NGC 2071 IR (at a much closer distance than G34.4), this work is presenting observations at a coarser resolution of $16''$. A larger beam may smear out the polarization P.A.s, erasing the outflow signature, which will produce a more uniform polarization pattern.

Both polarization results suggest a magnetic field perpendicular to the filament at different densities. The higher density MM core and UC H II region is traced by polarized dust

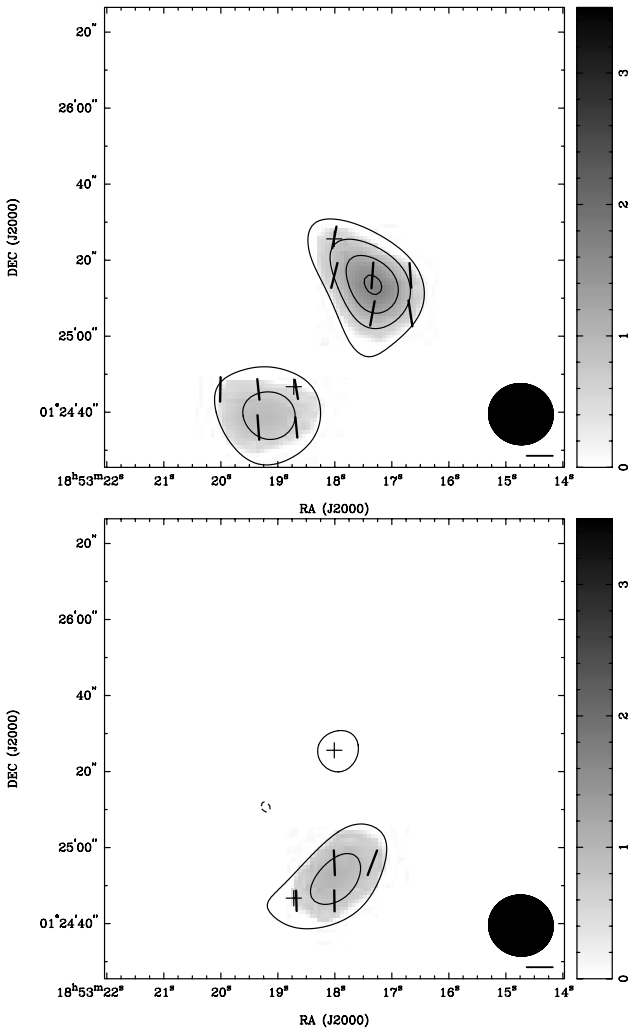

FIG. 6.— Redshifted (*top*) and blueshifted (*bottom*) emission as shown by Fig. 3, but with polarization maps superposed. The figure shows Stokes I as contours of -3, 3, 6, 9, and 12 σ, where $\sigma = 0.6$ Jy beam^{-1}. The small bar below the beam represents the fractional polarization scale in the map, corresponding to 0.22 for the red lobe and 0.25 for the blue lobe. The plus signs represent the positions of the MM core and the UC H II region.

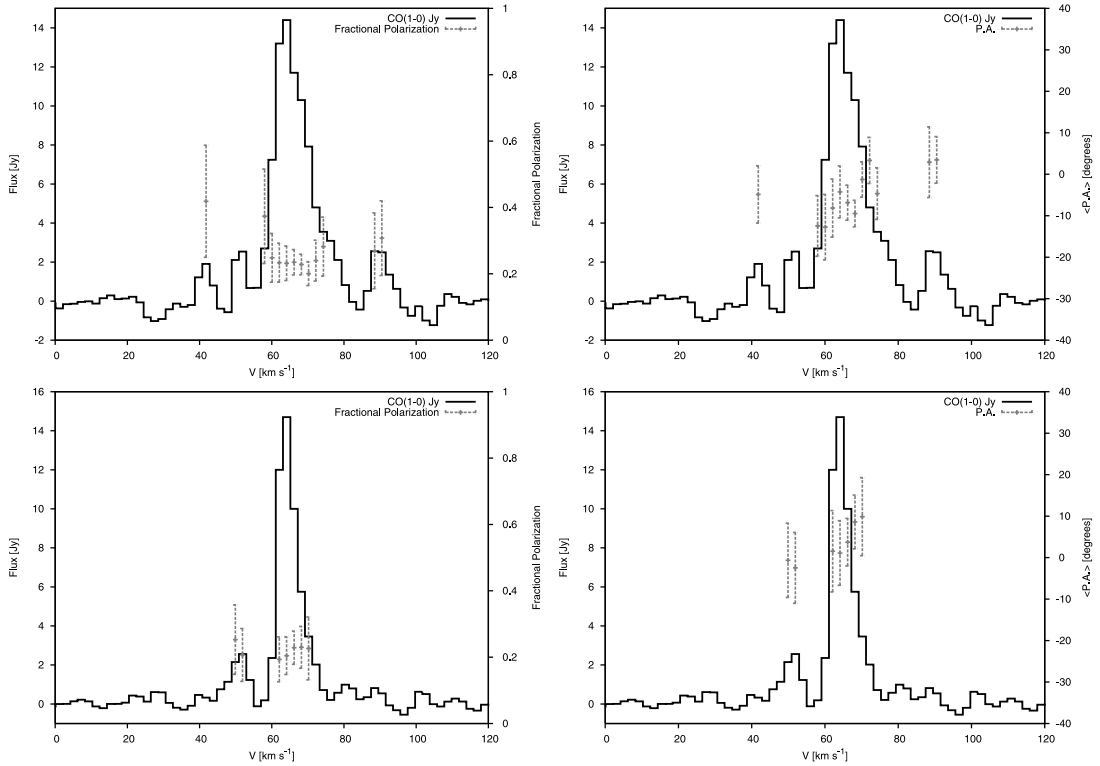

FIG. 7.— Two different spectra from the most intense CO $J = 1 \rightarrow 0$ emission points, which are averages taken in 8″ boxes centered at $(\alpha, \delta) = (18^{\rm h}53^{\rm m}17.3^{\rm s}, 01^{\circ}25'15'')$ and at $(18^{\rm h}53^{\rm m}19.2^{\rm s}, 01^{\circ}24'41'')$. The left panels have superposed the average fractional polarization values, while the right panels have average P.A. values.

emission, and the lower density cloud envelope or outflow extended region is traced by CO ($J = 1 \rightarrow 0$) polarized emission. It would be interesting to have higher resolution observations to map the polarized emission from the outflows in this region.

6. SUMMARY AND CONCLUSIONS

The G34.4+0.23 MM massive star-forming core was observed in the 3 mm band in polarized continuum and in CO $J = 1 \rightarrow 0$ polarized line emission with the BIMA array. The data show a uniform polarization pattern in both emissions. The P.A. obtained from the continuum data has an average value of $\langle\phi\rangle = -8^{\circ} \pm 5^{\circ}$, and from the CO polarization $\langle\phi\rangle = -2^{\circ} \pm 8^{\circ}$. These results suggest a magnetic field perpendicular to the main axis of the filament, between the MM source and the UC H II region, in G34.4. The morphology suggests a flattened disk with the magnetic field along the minor axis, as predicted by the theory of magnetically supported molecular clouds. From our 3 mm continuum observations, we estimate a total core mass of 400 $M_{\odot}$, in agreement with previous observations. Both line and continuum emission agrees in morphology with previous work by Shepherd et al. (2004, 2007). Finally, additional observations, particularly higher resolution interferometric mapping along the filament (including the most northern source seen in Fig. 1), will help to constrain in greater detail the morphology of the field and to obtain estimates of its strength in the plane of the sky.

P. C. Cortes acknowledges support from the ALMA-CONICYT fund for development of Chilean Astronomy through grant 31050003. P. C. Cortes would also like to acknowledge the support given by NCSA and the Laboratory for Astronomical Imaging at University of Illinois at Urbana-Champaign during this research. Finally, P. C. Cortes would like to acknowledge the contribution by Patricio Sanhueza in making Figure 1. R. M. Crutcher acknowledges support from NSF grants AST 05-40459 and 06-06822. L. Bronfman acknowledges support from the Chilean Center for Astrophysics FONDAP 15010003.

REFERENCES

Briggs, D. S., Schwab, F. R., & Sramek, R. A. 1999, in ASP Conf. Ser. 180, Synthesis Imaging in Radio Astronomy II, ed. G. B. Taylor, C. L. Carilli, & R. A. Perley (San Francisco: ASP), 127
Bronfman, L., Nyman, L.-A., & May, J. 1996, A&AS, 115, 81
Cortes, P., & Crutcher, R. M. 2006, ApJ, 639, 965
Cortes, P. C., Crutcher, R. M., & Matthews, B. C. 2006, ApJ, 650, 246
Cortes, P. C., Crutcher, R. M., & Watson, W. D. 2005, ApJ, 628, 780
Faúndez, S., Bronfman, L., Garay, G., Chini, R., Nyman, L.-Å., & May, J. 2004, A&A, 426, 97
Girart, J. M., Crutcher, R. M., & Rao, R. 1999, ApJ, 525, L109
Glenn, J., Walker, C. K., & Jewell, P. R. 1997, ApJ, 479, 325
Goldreich, P., & Kylafis, N. D. 1981, ApJ, 243, L75
Greaves, J. S., Holland, W. S., Friberg, P., & Dent, W. R. F. 1999, ApJ, 512, L139
Lai, S. P. 2001, Ph.D. thesis, Univ. Illinois, Urbana-Champaign
Lai, S., Crutcher, R. M., Girart, J. M., & Rao, R. 2002, ApJ, 566, 925
Lai, S., Girart, J. M., & Crutcher, R. M. 2003, ApJ, 598, 392
Lazarian, A. 2007, J. Quant. Spectrosc. Radiat. Transfer, 106, 225
Mezger, P. G. 1994, Ap&SS, 212, 197
Miralles, M. P., Rodriguez, L. F., & Scalise, E. 1994, ApJS, 92, 173
Molinari, S., Brand, J., Cesaroni, R., & Palla, F. 1996, A&A, 308, 573
Mooney, T., Sievers, A., Mezger, P. G., Solomon, P. M., Kreysa, E., Haslam, C. G. T., & Lemke, R. 1995, A&A, 299, 869
Palla, F., Brand, J., Comoretto, G., Felli, M., & Cesaroni, R. 1991, A&A, 246, 249
Ramesh, B., Bronfman, L., & Deguchi, S. 1997, PASJ, 49, 307
Rathborne, J. M., Jackson, J. M., Chambers, E. T., Simon, R., Shipman, R., & Frieswijk, W. 2005, ApJ, 630, L181
Rohlfs, K., & Wilson, T. L. 2004, Tools of Radio Astronomy (4th rev.; Berlin: Springer)

Sault, R. J., Teuben, P. J., & Wright, M. C. H. 1995, in ASP Conf. Ser. 77, Astronomical Data Analysis Software and Systems IV, ed. R. A. Shaw, H. E. Payne, & J. J. E. Hayes (San Francisco: ASP), 433
Scalise, E., Rodriguez, L. F., & Mendoza-Torres, E. 1989, A&A, 221, 105
Schleuning, D. A. 1998, ApJ, 493, 811
Schutte, A. J., van der Walt, D. J., Gaylard, M. J., & MacLeod, G. C. 1993, MNRAS, 261, 783
Shepherd, D. S., Nürnberger, D. E. A., & Bronfman, L. 2004, ApJ, 602, 850
Shepherd, D. S., Povich, M. S., Whitney, B. A., & Robitaille, T. P. 2007, ApJ, 669, 464
Szymczak, M., & Kus, A. J. 2000, A&AS, 147, 181